Bioorganic & Medicinal Chemistry 18 (2010) 5274–5281

Contents lists available at ScienceDirect

Bioorganic & Medicinal Chemistry

journal homepage: www.elsevier.com/locate/bmc

Development and evaluation of a ^{68}Ga labeled pamoic acid derivative for in vivo visualization of necrosis using positron emission tomography

Kristof Prinsen [a,*], Junjie Li [b], Hubert Vanbilloen [a], Peter Vermaelen [c], Ellen Devos [c], Luc Mortelmans [c], Guy Bormans [a], Yicheng Ni [b], Alfons Verbruggen [a]

[a] Laboratory for Radiopharmacy, Faculty of Pharmaceutical Sciences, Katholieke Universiteit Leuven, Herestraat 49, Box 821, BE-3000 Leuven, Belgium
[b] Department of Radiology, University Hospital Gasthuisberg, Katholieke Universiteit Leuven, Leuven, Belgium
[c] Department of Nuclear Medicine, University Hospital Gasthuisberg, Katholieke Universiteit Leuven, Leuven, Belgium

ARTICLE INFO

Article history:
Received 19 March 2010
Revised 15 May 2010
Accepted 18 May 2010
Available online 24 May 2010

Keywords:
Cell death
Necrosis
Gallium-68
PET

ABSTRACT

In this study, we labeled *N*,*N*′-bis(diethylenetriamine pentaacetic acid)-pamoic acid bis-hydrazide (bis-DTPA-PA) with the generator produced PET radionuclide gallium-68 and evaluated ^{68}Ga-bis-DTPA-PA as a potential tracer for in vivo visualization of necrosis by positron emission tomography (PET). Radiolabeling was achieved with a decay-corrected radiochemical yield of 63%. Biodistribution and in vivo stability studies in normal mice showed that ^{68}Ga-bis-DTPA-PA is cleared faster from normal tissue than the previously reported ^{99m}Tc(CO)$_3$ complex with bis-DTPA-PA which on the other hand is more stable in vivo. ^{68}Ga-bis-DTPA-PA showed a 3.5–5 times higher binding to necrotic tissue than to viable tissue as shown by in vitro autoradiography while no statistically significant increased hepatic uptake was found in a biodistribution study in a mouse model of hepatic apoptosis. Specificity and avidity for necrosis was further evaluated in rats with a reperfused partial liver infarction and ethanol induced muscular necrosis. Dynamic microPET images showed a fast and prolonged uptake of ^{68}Ga-bis-DTPA-PA in necrotic tissue with in vivo and ex vivo images correlating well with histochemical stainings. With necrotic to viable tissue activity ratios of 8–15 on ex vivo autoradiography, depending on the necrosis model, ^{68}Ga-bis-DTPA-PA showed a faster and higher uptake in necrotic tissue than the ^{99m}Tc(CO)$_3$ analog. These results show that ^{68}Ga-bis-DTPA-PA specifically binds to necrotic tissue and is a promising tracer for in vivo visualization of necrosis using PET.

1. Introduction

Cell death can result from two different but closely related processes, necrosis and apoptosis.[1–3] Apoptosis is a highly regulated, genetically defined and energy-dependent cellular process which can be initiated by several physiological stimuli. Once initiated, a preprogrammed set of cellular events, starting with activation of caspases, leads to a stereotyped series of morphological and biochemical changes resulting in a structured cell destruction and removal without invoking an inflammatory response. Apoptosis plays an essential role in organ development, tissue homeostasis and removal of defective cells and usually involves single cells. Defects in its control are involved in a variety of diseases.[4–6] Necrosis is the most frequent type of cell death and can be induced by a variety of sudden and severe non-physiological insults, including chemical or physical noxious insults and ischemic or inflammatory injury, as a result of which the normal homeostatic energy-dependent functions cannot occur. Necrotic cell death is characterized by progressive cell swelling, denaturation and coagulation of cytoplasmic proteins, disintegration of subcellular organelles, chromatin flocculation and irreversible loss of cell membrane integrity, leading to release of cytotoxic intracellular contents and a subsequent inflammatory response. In contrast to apoptosis, necrosis usually involves groups of cells and is frequently followed by development of replacement fibrosis with distortion of the local tissue's architecture.[2,3,7]

In pathological conditions, the two different types of cell death can occur simultaneously. Excessive cell death results in a progressive loss of tissue functionality, as occurs in acute myocardial infarction, chronic heart failure, allograft rejection, stroke, neurodegenerative disorders and inflammation.[8–13] On the other hand, a loss of normal apoptosis can lead to excessive cell proliferation and subsequent tumor development.[14,15] Today, the effect of many drugs can be attributed to their action on the cell death process and new therapies are often designed to prevent or induce cell death. Accordingly, in vivo monitoring of the rate and extent of cell death could provide relevant information on the therapeutic efficacy and disease activity and thereby assist in diagnosis and therapy management of several disorders.[16–18]

* Corresponding author. Tel.: +32 16 30446; fax: +32 16 330449.
E-mail address: kristof.prinsen@pharm.kuleuven.be (K. Prinsen).

0968-0896/$ - see front matter © 2010 Elsevier Ltd. All rights reserved.
doi:10.1016/j.bmc.2010.05.050

While molecular imaging of apoptosis using single photon emission computed tomography (SPECT) became a reality with the radiolabeling of annexin A5, a 36-kDa human protein that binds specifically to externalized phosphatidylserine with nanomolar affinity (K_d = 7 nM), molecular imaging of necrosis has proven to be a challenge given the fact that a multitude of substances are suddenly released by the dying cells following the loss of the cell membrane integrity.[19–21] ^{99m}Tc-pyrophosphate, ^{111}In-antimyosin Fab antibody, ^{99m}Tc-glucarate and mono-[^{123}I]iodohypericin have all been studied to non-invasively image necrosis but none has optimal imaging characteristics.[22,23]

While positron emission tomography (PET) with its higher sensitivity, better spatial resolution and the ability to better quantify the radiopharmaceutical uptake is superior to SPECT imaging, production of most PET tracers depends on the availability of an expensive on-site cyclotron for the production of short-lived radionuclides such as fluorine-18 ($t_{1/2}$ = 109.8 min) and carbon-11 ($t_{1/2}$ = 20.39 min). Gallium-68 (^{68}Ga) might overcome this shortcoming as it is produced from a ^{68}Ge/^{68}Ga generator, making ^{68}Ga supply independent from a cyclotron. ^{68}Ga has suitable physical properties for PET imaging with a high positron yield of 89% and a half-life of 68 min. The fact that it is produced from a generator with a long half-life of the parent isotope ($t_{1/2}$ ^{68}Ge = 270.8 days) makes it very cost-effective and available in-house for round the clock production of gallium-68 labeled tracer products.

Previously we reported that *N*,*N*′-bis(diethylenetriamine pentaacetic acid)-pamoic acid bis-hydrazide (bis-DTPA-PA; Fig. 1A) labeled with $^{99m}Tc(CO)_3^+$ or Gd^{3+} localizes in necrotic tissue in different animal models of necrosis.[24–26] Although the mechanism of uptake of these metal complexes of bis-DTPA-PA in necrotic tissue is still unknown, a possible hypothesis is that they bind to an intracellular protein which is exposed when the cell membrane integrity is lost during necrotic cell death. In this regard, pamoic acid has been reported as an inhibitor of DNA polymerase β, binding with a reasonable affinity to the 8-kDa subdomain of DNA polymerase β, that plays a central role in repair of damaged DNA bases.[27,28] Since DTPA can also form a complex with Ga^{3+} ($\log K_{ML}$ = 24.3)[29], bis-DTPA-PA can be labeled with the generator produced PET radionuclide ^{68}Ga and provide a necrosis-avid PET tracer. In the present study, we investigated the labeling of bis-DTPA-PA with ^{68}Ga and report the preliminary in vitro, ex vivo and in vivo evaluation of ^{68}Ga-bis-DTPA-PA as a necrosis-avid PET tracer.

2. Results and discussion

2.1. Radiochemistry

^{68}Ga was obtained by elution of a ^{68}Ge/^{68}Ga generator and the eluate was purified and concentrated following a reported procedure with some modifications.[30] Labeling of bis-DTPA-PA with ^{68}Ga was carried out in a sodium acetate buffer (pH ~ 4) by heating the labeling mixture at 90 °C for 5 min. Although DTPA can form a complex with ^{68}Ga at room temperature (RT), labeling at an elevated temperature resulted in faster incorporation of ^{68}Ga and higher radiochemical yields as compared to labeling at RT. The overall decay-corrected radiochemical yield was 63% with the entire procedure, including purification and concentration of ^{68}Ga, taking approximately 30 min. The radiochemical purity after purification of the crude labeling reaction mixture was found to be >99% using analytical reversed phase high performance liquid chromatography (RP-HPLC). Confirmation of the identity of ^{68}Ga-bis-DTPA-PA was obtained using radio-liquid chromatography–mass spectrometry (radio-LC–MS). Radio-LC–MS analysis of the reaction mixture after labeling of bis-DTPA-PA with ^{68}Ga in the presence of ^{69,71}Ga showed that the single radiometric peak is with high probability the desired compound, as the background-subtracted mass spectrum summed over this peak showed the presence of a molecular ion peak with a mass and isotopic distribution close to the theoretical mass and isotopic distribution of the desired ^{69,71}Ga complex of bis-DTPA-PA (Fig. 1B).

2.2. Distribution coefficient and protein binding measurements

The log distribution coefficient ($\log D$) value at pH 7.4 was −2.93 ± 0.03. The carboxylic acid functions of bis-DTPA-PA not participating in the complex formation—as only one gallium-68 ion is bound by a bis-DTPA-PA molecule in view of their molar ratios—account for the hydrophilic nature of the ^{68}Ga-bis-DTPA-PA complex, but this might not reflect the in vivo situation, where probably Ca^{2+} ions present in the blood will be complexed by the second DTPA-moiety, leading to an increased lipophilicity and potential retention. The protein binding results show that ^{68}Ga-bis-DTPA-PA very rapidly and strongly binds to human serum albumin (HSA) with 92.7 ± 2.1% and 93.6 ± 2.6% bound to HSA after 2 min and 30 min of incubation time, respectively. The interaction of the ^{68}Ga complex and previously reported $^{99m}Tc(CO)_3$ complex

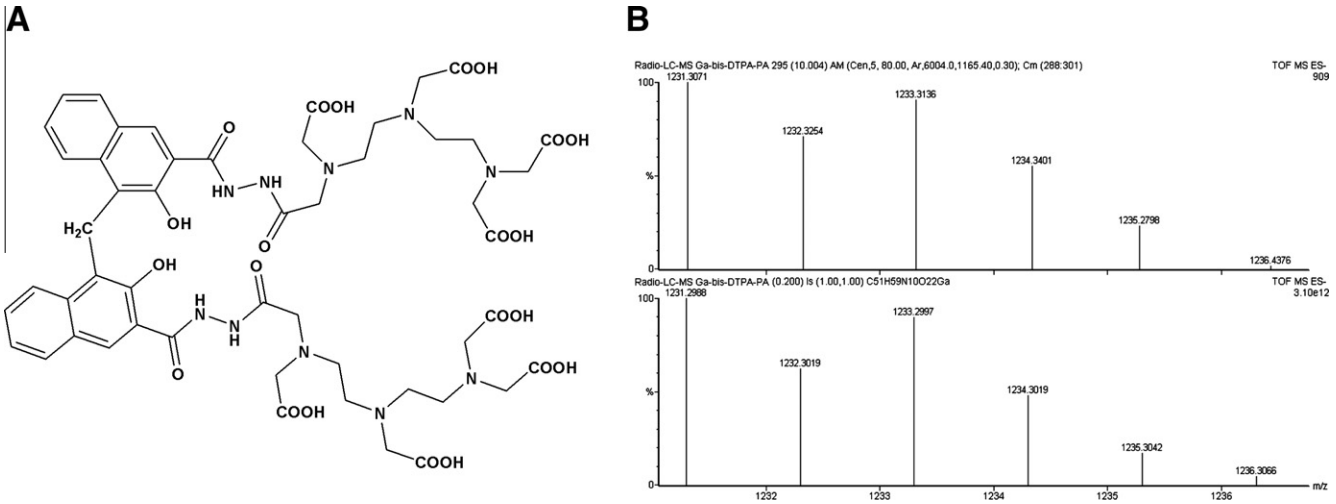

Figure 1. Chemical structure of bis-DTPA-PA (A). Accurate mass spectrum of ^{69,71}Ga-bis-DTPA-PA (B), the top spectrum shows the experimental mass spectrum whereas the bottom spectrum shows the theoretical mass spectrum.

(data not shown) with HSA could explain the long elimination half-life from the blood that was observed for both tracers in the biodistribution studies.[25]

2.3. Biodistribution in normal mice

The results of the biodistribution study of ^{68}Ga-bis-DTPA-PA in male NMRI mice at 30 min and 4 h post injection (pi) are shown in Table 1. The biodistribution of ^{68}Ga-bis-DTPA-PA was generally similar to the biodistribution of ^{99m}Tc(CO)$_3$-bis-DTPA-PA.[25] ^{68}Ga-bis-DTPA-PA was slowly cleared from the blood mainly via the renal pathway and to a lesser extent via the liver to the intestines. The clearance of ^{68}Ga-bis-DTPA-PA from blood was faster than that of ^{99m}Tc(CO)$_3$-bis-DTPA-PA with 5.8% versus 9.3% of injected dose/gram (% ID/g) of blood at 4 h pi for ^{68}Ga-bis-DTPA-PA and ^{99m}Tc(CO)$_3$-bis-DTPA-PA, respectively. In accordance with its ionized character at physiological pH and its log *D* value, ^{68}Ga-bis-DTPA-PA showed negligible brain uptake.

2.4. In vivo stability of ^{68}Ga-bis-DTPA-PA in normal mice

The in vivo stability of ^{68}Ga-bis-DTPA-PA was assessed in plasma col from male NMRI mice at 30 min or 4 h after injection of the tracer by determination of the relative amount of intact parent tracer using RP-HPLC. The obtained results are in line with the previously reported limited in vivo stability of the Ga-DTPA complex which leads to transchelation of Ga^{3+} to the blood protein transferrin.[31,32] Indeed, at 30 min pi, not more than 68.6 ± 2.8% of the recovered radioactivity in plasma was present as intact tracer and this decreased to 27.8 ± 3.2% at 4 h pi. The ^{99m}Tc(CO)$_3$ complex was more stable in vivo with 90% of the recovered radioactivity at 24 h pi present as intact tracer.[25]

2.5. In vitro autoradiography

As a first preliminary experiment to evaluate the avidity of ^{68}Ga-bis-DTPA-PA for necrosis, an in vitro autoradiography study was performed. Frozen sections (20 μm) of necrotic and viable liver tissue from a rat with a reperfused partial liver infarction were incubated with a solution of ^{68}Ga-bis-DTPA-PA for 10 min at RT and then exposed to a high performance phosphor screen to obtain autoradiographic images. Quantification of the in vitro autoradiographic images (comparison of digital light units (DLU) per square millimeter for necrotic and normal liver tissue) showed that ^{68}Ga-bis-DTPA-PA is avid for necrotic tissue with a 3.5–5 times higher binding of ^{68}Ga-bis-DTPA-PA to necrotic liver tissue as compared to the binding to viable liver tissue (Fig. 2).

Table 1
Biodistribution in normal NMRI mice ($n \geqslant 4$ per time point) of radioactivity after intravenous administration of ^{68}Ga-bis-DTPA-PA

Organ	% ID[a]		% ID/g[b]	
	30 min	4 h	30 min	4 h
Kidneys	7.2 ± 0.5	3.9 ± 0.7	13.8 ± 0.9	8.4 ± 0.8
Urine[c]	7.4 ± 6.6	25.2 ± 5.8		
Liver	6.7 ± 1.0	4.9 ± 0.9	3.4 ± 0.3	2.8 ± 0.3
Spleen and pancreas	0.8 ± 0.1	0.4 ± 0.0	2.8 ± 0.2	2.3 ± 0.3
Lungs	1.8 ± 0.5	0.9 ± 0.4	6.6 ± 1.0	3.7 ± 0.7
Heart	0.6 ± 0.1	0.3 ± 0.1	4.0 ± 0.7	2.3 ± 0.5
Intestines and feces[c]	7.1 ± 1.1	9.0 ± 0.7		
Stomach[c]	0.9 ± 0.3	1.1 ± 0.1		
Blood	25.3 ± 4.0	13.2 ± 3.5	11.3 ± 2.1	5.8 ± 1.2
Brain	0.1 ± 0.0	0.0 ± 0.0	0.2 ± 0.1	0.1 ± 0.0

Data are expressed as means ± SD.
[a] Percentage of injected dose calculated as cpm in tissue/total cpm recovered.
[b] Percentage of injected dose per gram tissue calculated as (cpm in tissue/total cpm recovered)/weight tissue in grams.
[c] Values are shown only as percentage of injected dose due to variability in the content of the bladder and gastrointestinal tract.

2.6. Biodistribution in mice with Fas-mediated hepatic apoptosis

To assess the specificity of ^{68}Ga-bis-DTPA-PA for necrosis and its ability to distinguish between necrotic and apoptotic cell death, the tracer was evaluated in a mouse model of hepatic apoptosis. In this mouse model, apoptosis is induced by treatment of the mice with FasL, a monoclonal antibody (mAb) directed against the Fas receptor. The Fas receptor is abundant in hepatocytes and binding of FasL to this receptor induces apoptosis resulting in massive apoptosis in the liver of FasL treated mice.[33,34] Comparison of the biodistribution of ^{68}Ga-bis-DTPA-PA in FasL treated and untreated male NMRI mice showed no statistically significant increased uptake of the tracer in the liver of FasL treated mice ($p > 0.05$; Fig. 3). These results show that ^{68}Ga-bis-DTPA-PA has no avidity for apoptotic cell death and can be considered specific for necrosis.

2.7. Small-animal PET studies

To study the kinetics and investigate the feasibility of in vivo visualization of necrosis using PET after injection of ^{68}Ga-bis-DTPA-PA, 4-h dynamic microPET images were acquired from rats with a reperfused partial liver infarction after administration of ^{68}Ga-bis-DTPA-PA. The high and steady activity in the kidneys observed on the time–activity curves (TACs) generated from the dynamic microPET images could be the result of the slow clearance

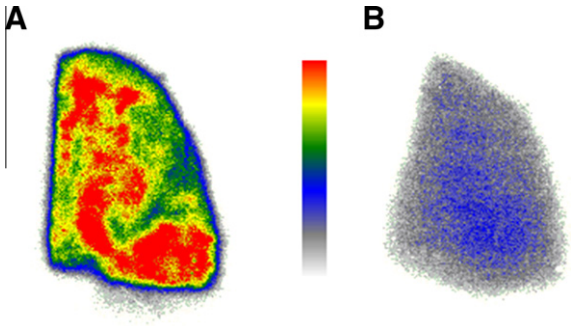

Figure 2. In vitro autoradiography of 20-μm necrotic (A) and viable (B) liver sections with ^{68}Ga-bis-DTPA-PA.

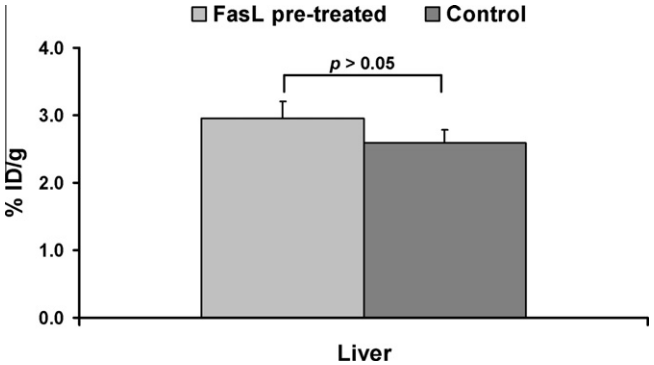

Figure 3. Comparison of the hepatic uptake of ^{68}Ga-bis-DTPA-PA 60 min pi in FasL treated mice ($n \geqslant 4$) and control mice ($n \geqslant 4$). Results are expressed as % of injected dose/gram of tissue (% ID/g) ± SD. *p* value shown for an unpaired *t*-test comparing FasL treated and control groups.

of the tracer from the blood (Fig. 4). TACs of the necrotic and viable liver lobes showed a fast uptake and prolonged retention of ^{68}Ga-bis-DTPA-PA in necrotic liver tissue while the tracer was cleared from the normal liver. While the necrotic liver lobe could clearly be distinguished from the viable liver lobes as early as 30 min pi of the tracer (Fig. 5), a maximum target-to-background activity ratio in necrotic tissue was reached at 90 min pi of ^{68}Ga-bis-DTPA-PA. Because the tracer is also cleared via the liver, microPET images were also acquired 1 h pi of ^{68}Ga-bis-DTPA-PA in rats with ethanol induced muscular necrosis in the right hind leg. The acquired images showed a clear uptake of the tracer in the area of muscular necrosis (muscle of right hind leg; injected with 0.2 mL EtOH) while no uptake was observed in the muscle of the left hind leg which was injected with 0.9% saline and served as a control (Fig. 6).

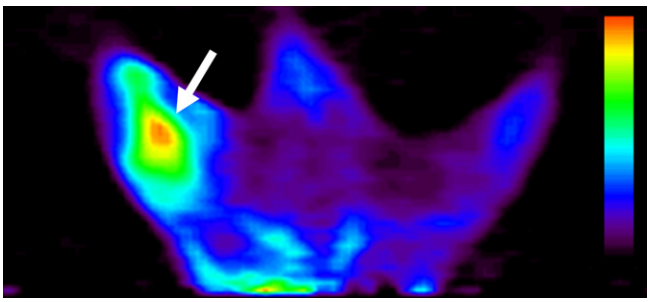

Figure 6. MicroPET image of a rat with ethanol induced muscular necrosis in the right hind leg 1 h pi of ^{68}Ga-bis-DTPA-PA. A high uptake of the tracer can be seen at the site of ethanol induced muscular necrosis (arrow).

2.8. Ex vivo autoradiography

Based on the TACs generated from the acquired dynamic microPET images, the specificity of ^{68}Ga-bis-DTPA-PA for necrosis was further evaluated ex vivo by autoradiography of tissue slices from rats with a reperfused partial liver infarction and rats with ethanol induced muscular necrosis at 90 min pi of ^{68}Ga-bis-DTPA-PA. Guided by triphenyltetrazolium chloride (TTC) staining, necrotic and viable liver tissue and muscle were selected and 10-, 30-, and 50-μm thick frozen sections of the selected tissue were exposed to a high performance phosphor screen. The presence or absence of necrosis was further confirmed using hematoxylin and eosin (H&E) staining in combination with microscopy techniques. Representative autoradiographic images of such tissue slices of a rat with a reperfused partial liver infarction are shown in Figure 7. Analysis of the autoradiographic images (comparison of the DLU/mm^2 for necrotic and normal tissue) showed that ^{68}Ga-bis-DTPA-PA was able to accurately delineate necrotic tissue with necrotic to viable tissue activity ratios of 8–10 on autoradiography for the liver and 12–15 for muscle. Although the obtained necrotic to viable tissue activity ratios for ^{68}Ga-bis-DTPA-PA are comparable to the ratios obtained with ^{99m}Tc(CO)$_3$-bis-DTPA-PA, it should be noted that these ratios are obtained at 90 min pi of ^{68}Ga-bis-DTPA-PA

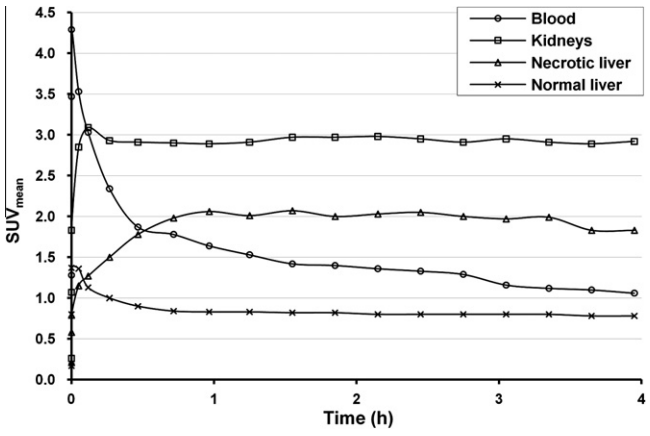

Figure 4. Time–activity curves in blood, kidneys, necrotic and viable liver lobes after iv injection of ^{68}Ga-bis-DTPA-PA in a rat with a reperfused partial liver infarction. ^{68}Ga-bis-DTPA-PA shows a fast uptake and prolonged retention in the necrotic tissue and reaches a maximum target-to-background activity ratio 90 min pi of the tracer.

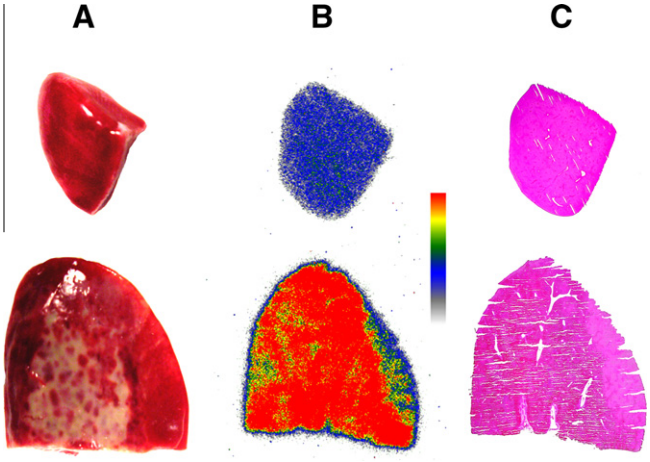

Figure 7. TTC stained liver lobes of a rat with a reperfused partial liver infarction 90 min pi of ^{68}Ga-bis-DTPA-PA (A); corresponding autoradiographic images (B) and H&E staining (C) of a 50-μm section of the viable (upper row) and necrotic (bottom row) liver lobe.

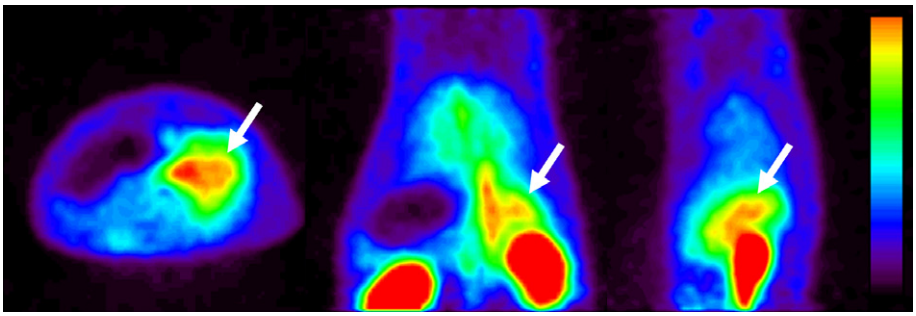

Figure 5. MicroPET image of a rat with a reperfused partial liver infarction in transverse (left), coronal (middle) and sagittal (right) views 30 min pi of ^{68}Ga-bis-DTPA-PA. A high uptake can be seen in the right necrotic liver lobes (arrow).

Table 2
Biodistribution of radioactivity 90 min pi of ^{68}Ga-bis-DTPA-PA in rats with a reperfused partial liver infarction ($n \geqslant 4$)

Organ	% ID/g[a] 90 min
Kidneys	1.9 ± 0.8
Viable liver lobe	0.4 ± 0.1
Necrotic liver lobe	1.4 ± 0.3
Spleen and pancreas	0.5 ± 0.1
Lungs	0.9 ± 0.1
Heart	0.6 ± 0.2
Blood	1.2 ± 0.1
Brain	0.0 ± 0.0
	% ID[b]
Stomach[c]	0.9 ± 0.3
Intestines and feces[c]	5.0 ± 1.5
Urine[c]	10.3 ± 7.1
Necrotic/viable tissue	3.4 ± 0.5
Necrotic tissue/blood	1.3 ± 0.2

Data are expressed as means ± SD.
[a] Percentage of injected dose per gram tissue calculated as (cpm in tissue/total cpm recovered)/weight tissue in grams.
[b] Percentage of injected dose calculated as cpm in tissue/total cpm recovered.
[c] Values are shown only as percentage of injected dose due to variability in the content of the bladder and gastrointestinal tract.

compared to 4 h pi of ^{99m}Tc(CO)$_3$-bis-DTPA-PA. This can be explained by the faster clearance of ^{68}Ga-bis-DTPA-PA from normal tissue observed in the biodistribution study.[25]

2.9. Biodistribution in rats with a reperfused partial liver infarction

To quantify the uptake of ^{68}Ga-bis-DTPA-PA in necrotic tissue, a biodistribution study in rats with a reperfused partial liver infarction was performed at 90 min pi of the tracer. The results (Table 2) showed a 3.4 ± 0.4 times higher uptake of ^{68}Ga-bis-DTPA-PA in necrotic liver tissue (1.4 ± 0.3% ID/g) as compared to the uptake in viable liver tissue (0.4 ± 0.1% ID/g). Comparison of these results with those reported for ^{99m}Tc(CO)$_3$-bis-DTPA-PA indicates that ^{68}Ga-bis-DTPA-PA has a faster and higher uptake in necrotic tissue than the ^{99m}Tc(CO)$_3$-labeled tracer.[25] The lower necrotic to viable tissue activity ratio obtained in the biodistribution study can be explained by the more accurate quantification of uptake in purely necrotic tissue by autoradiography whereas in the biodistribution study dissected necrotic tissue was always unavoidably mixed with some viable tissue.

3. Conclusions

In this study bis-DTPA-PA was labeled with the generator produced PET radionuclide gallium-68, characterized and evaluated in vitro, ex vivo and in vivo in different animal models of necrosis as a potential necrosis-avid PET tracer. The results show that ^{68}Ga-bis-DTPA-PA specifically binds to necrotic tissue and can accurately delineate necrotic tissue in vitro, ex vivo and in vivo. ^{68}Ga-bis-DTPA-PA can therefore be considered a potential radiopharmaceutical for in vivo visualization of necrosis using PET.

4. Experimental

4.1. General

N,*N*′-Bis(diethylenetriamine pentaacetic acid)-pamoic acid bis-hydrazide (bis-DTPA-PA) was synthesized as previously described.[25] Purified hamster anti-mouse CD95 mAb (FasL; Jo2 clone) was obtained from BD Pharmingen (Erembodegem, Belgium). Gallium-68 was obtained from a commercially available ^{68}Ge/^{68}Ga generator (Cyclotron Co., Obninsk, Russia). All other reagents and solvents were obtained commercially from Acros Organics (Geel, Belgium), Aldrich, Fluka or Sigma (Sigma–Aldrich, Bornem, Belgium) and used as supplied. High performance liquid chromatography (HPLC) analysis was performed on a system consisting of a Hitachi L-6200 intelligent pump connected to a Hitachi L-4200 UV detector (Hitachi, Tokyo, Japan) set at 254 nm. For analysis of radiolabeled compounds, after passing through the UV detector, the HPLC eluate was led over a 3-in. NaI(Tl) scintillation detector connected to a single-channel analyzer. The output signals were recorded and analyzed using a Laura Lite data acquisition system (version 3.0; Lablogic, Sheffield, UK). The radioactivity measurements for the log *D* determination, protein binding measurements, biodistribution studies and plasma analysis were done using an automatic gamma counter equipped with a 3-in. NaI(Tl) well crystal coupled to a multichannel analyzer (Wallac 1480 Wizard, Turku, Finland). The values were corrected for background radiation and physical decay during counting. Radio-LC–MS was performed on a system consisting of a Waters Alliance 2690 separation module (Waters, Milford, MA, USA) coupled to an XTerra® RP MS C_{18} column (3.5 μm, 2.1 mm × 50 mm; Waters). The column eluate was monitored using a Waters 2996 photodiode array detector (UV 200–500 nm; Waters) in series with a 3-in. NaI(Tl) detector connected to a single-channel analyzer (Raytest Gabi Star, Raytest Benelux B.V., Tilburg, The Netherlands). The column eluate was then directed to a time-of-flight mass spectrometer (Micromass LCT, Manchester, UK) equipped with an orthogonal electrospray ionization (ESI) probe. Acquisition and processing of the data was done using MassLynx™ software (version 3.5; Waters).

The animal studies were performed according to the Belgian code of practice for the care and use of animals, after approval from the university ethics committee for animals.

4.2. Radiochemistry

4.2.1. Purification and concentration of ^{68}Ga

^{68}Ga was obtained in the form of $^{68}GaCl_3$ from a ^{68}Ge/^{68}Ga generator by elution of the generator with 0.1 M HCl in three fractions (1.5, 6.0 and 4.5 mL). The second fraction (6.0 mL, containing >95% of the eluted activity) was mixed with 7.5 mL 37% HCl to obtain a final concentration of 5.5 M HCl in order to form $[^{68}GaCl_4]^-$. To concentrate the ^{68}Ga and remove any ^{68}Ge, which might be present in the generator eluate due to some breakthrough from the column, the mixture was transferred over a micro-chromatography column (20 mm × 3.0 mm) filled with a strong anion exchange resin (Dowex 1X8, 100–200 mesh; Dow Chemical, Midland, MI, USA) resulting in the adsorption of $[^{68}GaCl_4]^-$ on the micro-column. The micro-column was then washed with 3.0 mL of 5.5 M HCl and flushed with air to blow off most of the strong hydrochloric acid. Elution of ^{68}Ga from the micro-column was achieved with 0.8 mL of pure water, which leads to the decomposition of the $[^{68}GaCl_4]^-$ complex and release of ^{68}Ga as $^{68}Ga^{3+}_{aq}$.

4.2.2. Radiosynthesis of ^{68}Ga-bis-DTPA-PA

0.75 mL of a 0.5 M NaOAc buffer (pH 5.2) was added to the 0.8 mL concentrated ^{68}Ga solution to buffer the solution at pH ∼ 4. An amount of 20 nmol (23 μg) of bis-DTPA-PA was added to the buffered ^{68}Ga solution and the radiolabeling mixture was heated in an oil bath for 5 min at 90 °C. After cooling of the reaction mixture for 2 min, purification was achieved by loading it onto a solid phase extraction (SPE) cartridge (Strata-X C18-E 1 mL tubes; Phenomenex, Torrance, CA, USA) and washing the SPE cartridge with 3.0 mL water to remove any unbound ^{68}Ga. ^{68}Ga-bis-DTPA-PA was eluted from the SPE cartridge with 0.8 mL of ethanol and the eluate was collected in a septum-sealed glass vial. The ethanol

was evaporated by heating the glass vial in an oil bath at 55 °C under a stream of nitrogen for 10 min. Finally, ^{68}Ga-bis-DTPA-PA was dissolved in 1.0 mL 0.9% saline. The purified tracer was analyzed by HPLC on an analytical XTerra® RP C_{18} column (5 μm, 4.6 mm × 250 mm; Waters) eluted with gradient mixtures of 0.1% TFA in H_2O/0.1% TFA in acetonitrile (0 min: 100:0 v/v, 20 min: 10:90 v/v, linear gradient) at a flow rate of 1.0 mL/min.

4.2.3. Synthesis of ^{69,71}Ga-bis-DTPA-PA and radio-LC–MS analysis

0.75 mL of a 0.5 M NaOAc buffer (pH 5.2) was added to 0.8 mL concentrated ^{68}Ga solution to buffer the solution at pH ~ 4. An amount of 86 nmol (100 μg) of bis-DTPA-PA and $^{69,71}GaCl_3$ (0.57 mM, 150 μL, 86 nmol) was added to the buffered ^{68}Ga solution and the reaction mixture was heated at 90 °C for 5 min. The reaction mixture was analyzed by radio-LC–MS on an XTerra® RP MS C_{18} column eluted with gradient mixtures of 0.1% TFA in H_2O/0.1% TFA in acetonitrile (0 min: 100:0 v/v, 20 min: 10:90 v/v, linear gradient) at a flow rate of 0.2 mL/min. Electrospray ionization was performed in negative mode (ES−). In order to enable accurate mass calculations, a solution of a reference was used as an internal calibration standard. Accurate mass (ESI-MS) for $C_{51}H_{59}N_{10}O_{22}Ga$: found 1231.3071 Da, calculated 1231.2988 Da (retention time = 10.08 min).

4.2.4. Distribution coefficient and protein binding measurements

To determine the log distribution coefficient ($\log D_{n\text{-octanol/phosphate buffer pH 7.4}}$), an aliquot of 50 μL purified ^{68}Ga-bis-DTPA-PA in 0.9% saline was added to a tube containing 2.0 mL *n*-octanol (density = 0.827 g/mL) and 2.0 mL of 0.025 M sodium phosphate buffer pH 7.4 ($n \geqslant 6$). The tube was vortexed at RT for 2 min followed by centrifugation at 3000 rpm (1837 *g*) for 10 min (Eppendorf centrifuge 5810, Eppendorf, Westbury, NY, USA). Aliquots of 500 μL were drawn from the *n*-octanol phase and aqueous phase taking care to avoid cross-contamination between the two phases. The samples were weighed and the radioactivity was counted using an automatic gamma counter. After correcting for density and mass difference between the two phases, the distribution coefficient (*D*) was calculated as [radioactivity (cpm/mL) in *n*-octanol]/[radioactivity (cpm/mL) in phosphate buffer pH 7.4].

Protein binding of ^{68}Ga-bis-DTPA-PA was measured using an ultrafiltration method. To determine the percentage of ^{68}Ga-bis-DTPA-PA bound to human serum albumin (HSA), an aliquot of 50 μL purified ^{68}Ga-bis-DTPA-PA in 0.9% saline was added to a vial containing 1.0 mL of a 50 g/L HSA solution and the mixture was incubated at 37 °C ($n \geqslant 3$ per time point). At 2 min and 30 min after start of incubation, 200-μL aliquots were transferred to the pre-saturated sample reservoir of the ultrafiltration (UF) unit (Microcon Ultracel YM-10; MWCO 10 kDa; Millipore, Brussels, Belgium). The UF units were centrifuged at 14,000 *g* for 30 min at RT using a Galaxy 14D ultracentrifuge (VWR, Haasrode, Belgium). The tared filtrate collection tubes were weighed and the radioactivity present in the sample reservoir and in the filtrate was measured using an automatic gamma counter. To correct for non-specific binding, the experiment was repeated using a solution of ^{68}Ga-bis-DTPA-PA in 0.9% saline to determine the non-specific binding of ^{68}Ga-bis-DTPA-PA to the UF unit.

4.3. Biological studies

4.3.1. Biodistribution in normal mice

Biodistribution of ^{68}Ga-bis-DTPA-PA was studied in male NMRI mice (body mass 30–35 g). Mice were anesthetized with 2.0% isoflurane in O_2 at a flow rate of 1–2 L/min. Purified ^{68}Ga-bis-DTPA-PA solution was diluted with 0.9% saline to a concentration of approximately 3.7 MBq/mL or 29.6 MBq/mL (for 30 min or 4 h pi time points, respectively). A volume of 0.1 mL of the diluted purified tracer solution was then injected via a tail vein. Animals were sacrificed under anesthesia (isoflurane) by decapitation at 30 min or 4 h pi ($n \geqslant 4$ per time point). Blood and major organs were collected in tared tubes and weighed. The radioactivity in blood, organs, and other body parts was measured using an automatic gamma counter and the results were expressed as percentage of injected dose (% ID) or as percentage of injected dose per gram tissue (% ID/g). For calculation of total blood radioactivity, blood mass was assumed to be 7% of the total body mass.[35]

4.3.2. In vivo stability of ^{68}Ga-bis-DTPA-PA in normal mice

In vivo stability of ^{68}Ga-bis-DTPA-PA after intravenous (iv) injection in male NMRI mice was assessed by HPLC analysis of plasma at 30 min or 4 h pi ($n \geqslant 2$ per time point) by using an Oasis® HLB column (Hydrophilic-Lipophilic Balanced; 25 μm, 4.6 mm × 250 mm; Waters) in series with an analytical XTerra® RP C_{18} column (5 μm, 4.6 mm × 250 mm; Waters).[36] After iv injection of 5.55–14.8 MBq ^{68}Ga-bis-DTPA-PA via a tail vein, mice were sacrificed under anesthesia (isoflurane) by decapitation. Blood was collected into BD vacutainer® tubes (containing 7.2 mg K_2EDTA; Beckton–Dickinson, Franklin Lakes, NJ, USA) and stored on ice. Samples were then centrifuged at 3000 rpm (1837 *g*) for 5 min (Eppendorf centrifuge 5810) in order to separate plasma. A volume of 0.5 mL of plasma sample was injected onto an Oasis® HLB column that was preconditioned by successive washings with acetonitrile and water. The proteins and other biological matrices were washed off the Oasis® HLB column with 6.0 mL of water, which was collected in 6 × 1.0-mL fractions. The outlet of the Oasis® HLB column was then connected to an analytical XTerra® RP C_{18} column, and both columns in series were eluted using gradient mixtures of 0.1% TFA in H_2O/0.1% TFA in acetonitrile (0 min: 100:0 v/v, 20 min: 10:90 v/v, linear gradient) at a flow rate of 1.0 mL/min. The HPLC eluate was collected in 20 × 1.0-mL fractions and the radioactivity was measured using an automatic gamma counter.

4.3.3. Animal models of necrosis

4.3.3.1. Rat model of reperfused partial liver infarction.

Wistar rats (body mass 250–300 g, 8 weeks old, male) were anesthetized with an intraperitoneal injection (ip) of pentobarbital (40 mg/kg; Sanofi Santé Animale, Brussels, Belgium). Under laparotomy, a reperfused partial liver infarction was induced by clamping of the hilum of the right liver lobes for 3 h. After reperfusion by declamping the hepatic inflow, the abdominal cavity was closed with two-layered sutures, and the animals were allowed to recover for 8–12 h after the surgery, as detailed elsewhere.[37]

4.3.3.2. Rat model of ethanol induced muscular necrosis.

Wistar rats (body mass 250–300 g, 8 weeks old, male) were anesthetized as described above. Muscular necrosis was induced by gradual infusion of 0.2 mL ethanol into the muscle of the right hind limb of the animal, the muscle of the left hind limb was injected with 0.9% saline and served as a control. Animals were allowed to recover for 8–12 h after the procedure.

4.3.4. Mouse model of Fas-mediated hepatic apoptosis

Male NMRI mice (body mass 30–35 g) were anesthetized with isoflurane and injected via a tail vein with purified hamster anti-mouse CD95 mAb (FasL; 0.2 mg/kg).

4.3.5. In vitro autoradiography

For in vitro autoradiography studies, a rat with a reperfused partial liver infarction was sacrificed with an ip overdose of pentobarbital. The liver was removed and thoroughly washed with 0.9% saline (4 °C). Necrotic and viable liver tissue was rapidly frozen in

isopentane cooled with liquid nitrogen to −50 °C and cut with a cryotome (Shandon Cryotome FSE; Thermo Fisher, Waltham, MA, USA). Twenty micrometer thick serial sections were thaw-mounted on glass slides, which were then dried for 30 min at RT, fixed in acetone for 10 min (−20 °C) and stored at −20 °C until used for experiments. Sections of viable ($n \geqslant 6$) and necrotic liver tissue ($n \geqslant 6$) were pre-incubated at RT for 10 min in 50 mM Tris–HCl buffer (pH 7.4) containing 0.1% bovine serum albumin (BSA). After pre-incubation each section was incubated for 10 min at RT with 300 μL assay buffer containing ^{68}Ga-bis-DTPA-PA (740 kBq/mL in 50 mM Tris–HCl buffer pH 7.4 containing 0.1% BSA) and then rinsed twice (2 × 5 min) with 50 mM Tris–HCl buffer pH 7.4 containing 0.1% BSA at 4 °C. After a quick dip in water at RT, the sections were dried. Autoradiographic images were obtained by exposing the sections overnight to a high performance phosphor screen (super resolution screen; Canberra-Packard, Meriden, CT, USA). Images were obtained by reading the phosphor screen using a Cyclone Phosphor Imager scanner (Canberra-Packard) and analyzed with Optiquant software (version 5.0; Canberra-Packard). The radioactivity concentration in the autoradiographic images was expressed in digital light units (DLU) per square millimeter (DLU / mm^2). Relative tracer concentrations in the necrotic and viable tissue sections were estimated by regions of interest (ROI) analysis of the autoradiographic images. After exposure for autoradiography, the sections were stained with hematoxylin and eosin using a conventional procedure and examined under a microscope to confirm the presence or absence of necrosis.

4.3.6. Biodistribution in mice with Fas-mediated hepatic apoptosis

To investigate the specificity of ^{68}Ga-bis-DTPA-PA for necrosis, biodistribution of ^{68}Ga-bis-DTPA-PA was studied in a mouse model of hepatic apoptosis and compared to the biodistribution of ^{68}Ga-bis-DTPA-PA in untreated mice at the same time point. Male NMRI mice (body mass 30–35 g; $n \geqslant 4$) and FasL treated mice (body mass 30–35 g; $n \geqslant 4$; 90 min pi of 0.2 mg/kg FasL) were anesthetized (isoflurane) and injected with 370 kBq of purified ^{68}Ga-bis-DTPA-PA in 0.1 mL 0.9% saline via a tail vein. Mice were sacrificed by decapitation under anesthesia (isoflurane) 60 min pi of the tracer. Blood and major organs were collected in tared tubes and weighed. The radioactivity in blood, organs and other body parts was measured using an automatic gamma counter and the results were expressed as percentage of injected dose per gram tissue (% ID/g). For the calculation of total blood radioactivity, blood mass was assumed to be 7% of the total body mass.[35] Statistical significance was tested by an unpaired *t*-test using GraphPad (version 4.0; GraphPad, San Diego, CA, USA). *p* values <0.05 were considered statistically significant.

4.3.7. Small-animal PET studies

MicroPET images were acquired on a FOCUS 220 tomograph (Siemens/Concorde Microsystems, Knoxville, USA). Rats were anesthetized with isoflurane (1.5–2.5% in oxygen; flow rate of 1–2 L/min) and fixed in prone position on the bed of the small-animal PET tomograph. MicroPET images of rats with a reperfused partial liver infarction ($n \geqslant 3$) were acquired, after administration of purified ^{68}Ga-bis-DTPA-PA (55.5 MBq in 0.5 mL 0.9% saline) as a bolus injection via a tail vein, using a 51-dynamic frame protocol (4 h total; 4 × 15 s, 4 × 60 s, 5 × 180 s, 8 × 300 s, 30 × 360 s). MicroPET images were reconstructed using a 2D OSEM algorithm. Data were analyzed using PMOD (version 2.65; PMOD Inc., Zurich, Switzerland). Mean images were created and used to define volumes of interest (VOIs) on the microPET images in order to generate TACs. MicroPET images of rats with ethanol induced muscular necrosis ($n \geqslant 3$) were acquired 1 h pi of ^{68}Ga-bis-DTPA-PA (27.8 MBq in 0.5 mL 0.9% saline, bolus injection) via a tail vein using a 10-min static acquisition protocol. Images were reconstructed using a 2D OSEM algorithm and analyzed using PMOD.

4.3.8. Ex vivo autoradiography

For ex vivo autoradiography studies, rats with a reperfused partial liver infarction ($n \geqslant 3$) were anesthetized with isoflurane and 55.5 MBq of purified ^{68}Ga-bis-DTPA-PA in 0.5 mL 0.9% saline was injected via a tail vein. Ninety minutes pi of the tracer, the rats were sacrificed as described above. The liver was removed and washed thoroughly with 0.9% saline (4 °C) to remove blood pool activity. Necrotic and viable liver tissue were stained separately in a TTC solution (1.5% w/v in 0.9% saline) at 37 °C for 10 min to visually confirm the presence (unstained) or absence (stained red) of necrosis. The tissue samples were then rapidly frozen as described above and cut with a cryotome (Shandon Cryotome FSE) into 10-, 30- and 50-μm thick serial sections and thaw-mounted on glass slides. Autoradiographic images were obtained and analyzed as described above. The tissue sections were histochemically stained and examined as described above.

4.3.9. Biodistribution in rats with a reperfused partial liver infarction

Biodistribution of ^{68}Ga-bis-DTPA-PA was studied in rats with a reperfused partial liver infarction. Rats ($n \geqslant 4$) were anesthetized (isoflurane) and 11.1 MBq of purified ^{68}Ga-bis-DTPA-PA in 0.5 mL 0.9% saline was injected via a tail vein. Ninety minutes pi of the tracer the rats were sacrificed with an ip overdose of pentobarbital. Necrotic and viable liver tissue, blood, major organs and other body parts were collected in tared tubes and weighed. The radioactivity present in necrotic liver tissue, viable liver tissue, blood, major organs and other body parts was measured using an automatic gamma counter and the results were expressed as percentage of injected dose per gram tissue (% ID/g).

Acknowledgments

The authors thank Ann Van Santvoort for her skillful help with the animal experiments and small-animal PET imaging studies. Research funded by a Ph.D. grant of the Institute for the Promotion of Innovation through Science and Technology in Flanders (IWT-Vlaanderen). This research was further supported by the Euregional PACT Project EFRO-INTERREG-EUROPACT II: IVA-VLANED-1.20 and the DiMI Project DiMI-EU-FP6: SHB-CT-2005-512146.

References and notes

1. Kerr, J. F.; Wyllie, A. H.; Currie, A. R. *Br. J. Cancer* **1972**, *26*, 239.
2. Majno, G.; Joris, I. *Am. J. Pathol.* **1995**, *146*, 3.
3. McConkey, D. J. *Toxicol. Lett.* **1998**, *99*, 157.
4. Wyllie, A. H.; Kerr, J. F. R.; Currie, A. R. *Int. Rev. Cytol.* **1980**, *68*, 251.
5. Hetts, S. W. *JAMA* **1998**, *279*, 300.
6. Honig, L. S.; Rosenberg, R. N. *Am. J. Med.* **2000**, *108*, 317.
7. Proskuryakov, S. Y.; Konoplyannikov, A. G.; Gabai, V. L. *Exp. Cell Res.* **2003**, *283*, 1.
8. Braunwald, E.; Kloner, R. A. *J. Clin. Invest.* **1985**, *76*, 300.
9. Kajstura, J.; Cheng, W.; Reiss, K.; Clark, W. A.; Sonnenblick, E. H.; Krajewski, S.; Reed, J. C.; Olivetti, G.; Anversa, P. *Lab. Invest.* **1996**, *74*, 86.
10. Ballester, M.; Obrador, D.; Carrio, I.; Auge, J. M.; Moya, C.; Pons-Llado, G.; Caralps-Riera, J. M. *Circulation* **1990**, *82*, 2100.
11. Garcia, J. H.; Liu, K. F.; Ho, K. L. *Stroke* **1995**, *265*, 636.
12. Garcia, J. H.; Lassen, N. A.; Weiller, C.; Sperling, B.; Nakagawara, J. *Stroke* **1996**, *27*, 761.
13. Mareninova, O. A.; Sung, K. F.; Hong, P.; Lugea, A.; Pandol, S. J.; Gukovsky, I.; Gukovskaya, A. S. *J. Biol. Chem.* **2006**, *281*, 3370.
14. Kerr, J. F. R.; Winterford, C. M.; Harmon, B. V. *Cancer* **1994**, *73*, 3018.
15. Lowe, S. W.; Lin, A. W. *Carcinogenesis* **2000**, *21*, 485.
16. Blankenberg, F. G.; Narula, J.; Strauss, H. W. *J. Nucl. Cardiol.* **1999**, *6*, 531.
17. Green, A. M.; Steinmetz, N. D. *Cancer J.* **2002**, *8*, 82.
18. Perek, N.; Sabido, O.; Le Jeune, N.; Prevot, N.; Vergnon, J. M.; Clotagide, A.; Dubois, F. *Eur. J. Nucl. Med. Mol. Imaging* **2008**, *35*, 1290.
19. Lahorte, C. M.; Vanderheyden, J. L.; Steinmetz, N.; Van de Wiele, C.; Dierckx, R. A.; Slegers, G. *Eur. J. Nucl. Med. Mol. Imaging* **2004**, *31*, 887.

20. Boersma, H. H.; Kietselaer, B. L.; Stolk, L. M.; Bennaghmouch, A.; Hofstra, L.; Narula, J.; Heidendal, G. A.; Reutelingsperger, C. P. *J. Nucl. Med.* **2005**, *46*, 2035.
21. Hofstra, L.; Liem, I. H.; Dumont, E. A.; Boersma, H. H.; van Heerde, W. L.; Doevendans, P. A.; De Muinck, E.; Wellens, H. J.; Kemerink, G. J.; Reutelingsperger, C. P.; Heidendal, G. A. *Lancet* **2000**, *356*, 209.
22. Flotats, A.; Carrió, I. *Eur. J. Nucl. Med. Mol. Imaging* **2003**, *30*, 615.
23. De Saint-Hubert, M.; Prinsen, K.; Mortelmans, L.; Verbruggen, A.; Mottaghy, F. M. *Methods* **2009**, *48*, 178.
24. Ni, Y.; Bormans, G.; Chen, F.; Verbruggen, A.; Marchal, G. *Invest. Radiol.* **2005**, *40*, 526.
25. Fonge, H.; Chitneni, S. K.; Lixin, J.; Vunckx, K.; Prinsen, K.; Nuyts, J.; Mortelmans, L.; Bormans, G.; Ni, Y.; Verbruggen, A. *Bioconjugate Chem.* **2007**, *18*, 1924.
26. Marchal, G. J. F.; Verbruggen, A.; Ni, Y.; Adriaens, P. Patent PCT/BE99/00104, 2000.
27. Hu, H. Y.; Horton, J. K.; Gryk, M. R.; Prasad, R.; Naron, J. M.; Sun, D. A.; Hecht, S. M.; Wilson, S. H.; Mullen, G. P. *J. Biol. Chem.* **2004**, *279*, 39736.
28. Hazan, C.; Boudsocq, F.; Gervais, V.; Saurel, O.; Caias, M.; Cazaux, C.; Czaplicki, J.; Milon, A. *BMC Struct. Biol.* **2008**, *8*, 22.
29. Smith, R. M.; Martell, A. E.; Motekaitis, R. J. *Critical Stability Constants Database 46*; NIST: Gaithersburg, 1993.
30. Meyer, G. J.; Mäcke, H.; Schuhmacher, J.; Knapp, W. H.; Hofmann, M. *Eur. J. Nucl. Med. Mol. Imaging* **2004**, *31*, 1097.
31. Wagner, S. J.; Welch, M. J. *J. Nucl. Med.* **1979**, *20*, 428.
32. Smith-Jones, P. M.; Stolz, B.; Bruns, C.; Albert, R.; Reist, H. W.; Fridrich, R.; Maecke, H. R. *J. Nucl. Med.* **1994**, *35*, 317.
33. Blankenberg, F. G.; Katsikis, P. D.; Tait, J. F.; Davis, R. E.; Naumovski, L.; Ohtsuki, K.; Kopiwoda, S.; Abrams, M. J.; Strauss, H. W. *J. Nucl. Med.* **1999**, *40*, 184.
34. Ogasawara, J.; Watanabe-Fukunaga, R.; Adachi, M.; Matsuzawa, A.; Kasugai, T.; Kitamura, Y.; Itoh, N.; Suda, T.; Nagata, S. *Nature* **1993**, *364*, 806.
35. Fritzberg, A. R.; Whitney, W. P.; Kuni, C. C.; Klingensmith, W. *Int. J. Nucl. Med. Biol.* **1982**, *9*, 79.
36. Chitneni, S. K.; Serdons, K.; Evens, N.; Fonge, H.; Celen, S.; Deroose, C. M.; Debyser, Z.; Mortelmans, L.; Verbruggen, A. M.; Bormans, G. M. *J. Chromatogr., A* **2008**, *1189*, 323.
37. Wu, X.; Wang, H.; Chen, F.; Jin, L.; Li, J.; Feng, Y.; Dekeyzer, F.; Yu, J.; Marchal, G.; Ni, Y. *Acta Radiol.* **2009**, *50*, 276.